

Obtaining Creep Compliance from BBR Tests on Mixture Beams

Previous research performed at the University of Minnesota (2, 3, 4, 5, 6,7, 8) showed that the Bending Beam Rheometer (BBR), currently used for asphalt binders specifications, can be used to obtain creep properties of asphalt mixtures, see Figure 31.

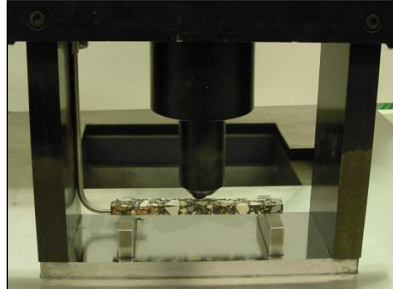


Figure 31. Bending Beam Rheometer with beam of asphalt mixture

The main difficulty in implementing this method into current practice is the use of small size specimens that may not capture the mechanical behavior of the actual asphalt pavement, see Figure 2. The volume of material tested may not be representative, especially when the asphalt mixtures contained aggregate sizes that are larger than the smallest dimension of the beam.



Figure 32. IDT and BBR test specimens

Work performed in a recent NCHRP Idea project investigated the feasibility of using the BBR for asphalt mixture characterization by means of creep tests, image analysis, microstructure characterization with spatial correlation functions, and finite element simulations of specimens of different sizes. A summary of the results is presented in the next paragraphs.

Experimental work

A total of 360 three-point bending creep tests were performed on three beam sizes: $6.25 \times 12.5 \times 100$ mm (1x), $12.5 \times 25 \times 200$ mm (2x), and $18.75 \times 37.5 \times 300$ mm (3x). The bending creep test were performed at three temperatures: high temperature (HT) level (PG low limit + 22°C), intermediate temperature (IT) level (PG low limit + 10°C), and low temperature (LT) level (PG low limit - 2°C). The PG low limit is the low temperature performance grade limit of the asphalt

binder. Three replicates were tested at high temperature level (HT) and low temperature level (LT) and six replicates were tested at intermediate temperature level (IT).

A total of ten laboratory prepared mixtures were tested. The mixtures were selected from the set of mixtures used in the first phase of the pooled fund study, and were prepared using four asphalt binder grades, and two types of aggregate: limestone and granite. They were compacted to 4% air voids using a linear kneading compactor. The mixing and compaction temperatures were 155°C and 135°C, respectively. Figure 33 shows the gradation curves of the granite and limestone aggregates used for asphalt mixture preparation. The particle size distribution curves for granite and limestone are very similar with a maximum aggregate size of 12.5 mm. The percent of material passing sieve #200 (i.e. 75 µm) is 5.1 and 5.4% for granite and limestone, respectively.

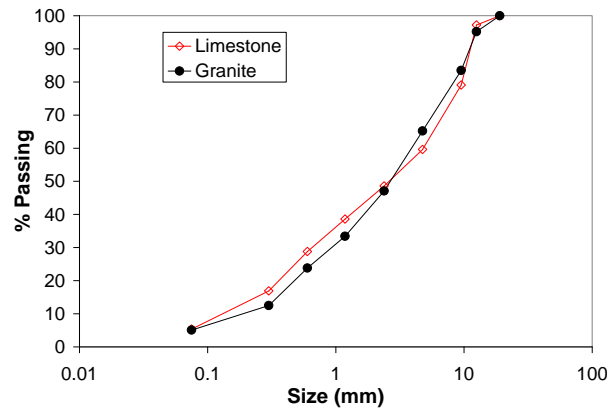


Figure 33. Gradation curves for granite and limestone aggregate

Table 5 contains a description of the ten asphalt mixtures tested, including the performance grade (PG) of the binder, modification, and type of aggregate.

Table 5. Description of asphalt mixtures

ID	PG binder	Modification	Aggregate
58-34:M2:4:GR	58-34	SBS	Granite
58-34:M2:4:LM	58-34	SBS	Limestone
58-28:U1:4:GR	58-28	Unmodified	Granite
58-28:U1:4:LM	58-28	Unmodified	Limestone
64-34:M1:4:GR	64-34	Elvaloy	Granite
64-34:M1:4:LM	64-34	Elvaloy	Limestone
64-28:U1:4:GR	64-28	Unmodified	Granite
64-28:U1:4:LM	64-28	Unmodified	Limestone
64-28:M1:4:GR	64-28	SBS	Granite
64-28:M1:4:LM	64-28	SBS	Limestone

The slab compacted mixtures were cut into 3x beams (18.75 × 37.5 × 300 mm) as shown in Figure 34. After testing was finished, the 3x beams were cut into 2x beams (12.5 × 25 × 200 mm) using a typical laboratory diamond saw. After completion of the testing of the 2x beams,

specimens were cut into 1x beams (6.25 × 12.5 × 100 mm), which is the size of Bending Beam Rheometer (BBR) specimens.

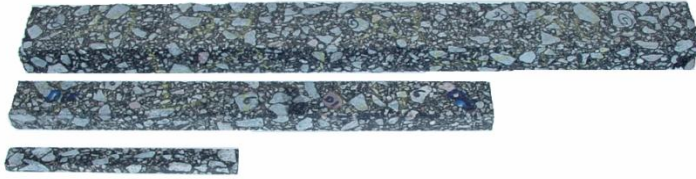


Figure 34. 1x, 2x, and 3x asphalt mixture beam specimens

The thickness and width of the 3x, 2x, and 1x beams were measured at three locations along the length of the beam and average values were used in the calculation of the creep stiffness. A summary of basic statistical parameters of the measured dimensions, weight, and density is presented in Table 6. The coefficient of variation for width, thickness, length, and weight for the 3x, 2x and 1x beams indicate that specimens are uniform and very consistent. The 95% confidence intervals for the thickness, width, and density indicate that the variation of the dimensions of the 3x, 2x, and 1x beams are insignificant.

Table 6. Statistical summary for dimensions of 3x, 2x, and 1x beams

	3x		2x		1x	
	μ	CV(%)	μ	CV(%)	μ	CV(%)
width (mm)	37.91	2.44	25.05	3.16	12.43	1.25
thickness (mm)	19.32	2.04	12.62	3.15	6.65	4.10
length (mm)	383.00	0.24	257.27	0.28	126.58	0.59
weight (gr)	622.96	5.26	183.41	4.87	23.43	5.12
ρ (gr/cm³)	2.22	4.16	2.26	4.45	2.24	5.11

The three-point bending tests for 3x and 2x beams were conducted using a MTS 810 servo hydraulic load frame. A special support manufactured in-house was used to hold the beam and to allow measurements of mid span deflection. The beam deflections were measured using Epsilon extensometers with 38 mm gage length and ±1 mm range. The thin asphalt concrete beams (1x) were tested with the Bending Beam Rheometer (BBR) following the procedure described in detailed in (8).

The creep stiffness as a function of time was calculated using Euler- Bernoulli beam theory and the correspondence principle. For each mixture and temperature level, the average creep stiffness was calculated by:

$$S(t) = \frac{L^3}{48\delta(t)I} \left[P + \frac{5wL}{8} \right] \quad (1)$$

where,

S = creep stiffness

P = constant load applied to the beam

L = span length

I = moment of inertia of the beam

$\delta(t)$ = deflection of the beam

w = uniformly distributed load due to weight of the beam

Due to the buoyancy forces in the BBR ethanol bath, the submerged weight for the 1x beams was negligible and not used in equation 1.

Figure 35 shows an example of the creep stiffness curves for the ten mixtures tested. All creep stiffness curves can be found in (7). Visual inspection of the creep stiffness average curves indicates that, at intermediate and high temperature, the effect of the beam size is negligible.

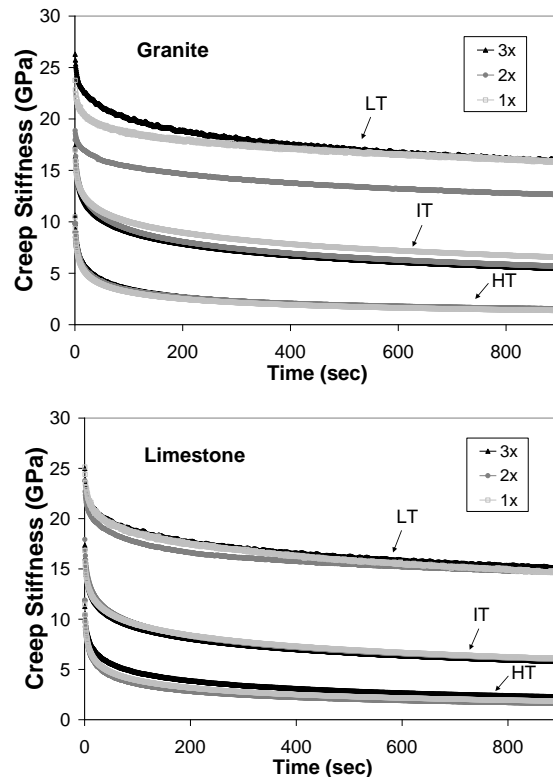


Figure 35. Test results for PG 58-34 mixtures

The experimental results at the high and intermediate temperature levels (HT and IT) indicate that the average information contained in the 1x beams ($6.25 \times 12.5 \times 100$ mm) is statistically representative of the material, even though the mixtures contain aggregate sizes (i.e. 12.5 mm) which are larger than the smallest dimension of the beam.

At low temperature, the size of the beam appears to influence the creep stiffness. However, it is important to note that, during testing of the 2x and 3x beams at the low temperature level (LT), the formation of layers of ice on the supports and around the extensometers was observed. This may have influenced the deflection readings, since the deflection values are very small at LT and the level of error in measurements is higher compared to the other temperature levels.

To investigate the influence of parameters such as the size of the specimen, performance grade (PG) of the binder, aggregate type, loading time, and temperature on the creep stiffness of asphalt mixtures, correlation matrices were calculated and analyses of variance (ANOVA) were

performed using the creep stiffness as response variable and size, time, temperature, binder type, and aggregate as the independent parameters. A linear relation was assumed between response variable and the predictors. To reduce calculations, only the creep stiffness values at 8, 15, 30, 60, 120, and 240 seconds were used in the analysis. Table 7 shows how the variables were treated in the statistical analysis.

Table 7. Variables definition for statistical analysis

Variable	Type / Description
Binder PG	Factors (dummy): PG 58-34, PG 58-28, PG 64-34, PG 64-28
Binder modification	0 – unmodified; 1 – modified
Aggregate Type	0 – granite; 1 – limestone
Beam size	1 – 1x beams; 2 - 2x beams; 3 - 3x beams
Time	8, 15, 30, 60, 120 and 240 sec

The creep stiffness data from the low temperature level was not included in the statistical analysis due to the poor quality and high variability of the deflection measurements obtained. The formation of layers of ice between supports and the sample, the variability of the extensometers readings at this temperature, and the brittleness of the specimens are explanations on the level of error observed at this temperature level.

Correlation factors for the results obtained at intermediate and high temperatures are presented in Table 8. Correlation factors more than $2/n^{0.5}$ (**9**), where n is the number of sample points, indicates high linear correlation between the parameters. For the data set used in this analysis, correlations larger than 0.057 ($n = 1225$) are significant and presented in bold.

Table 8. Correlation factors for all temperatures

	Creep Stiffness
Aggregate	0.128
Modification	-0.123
Size	-0.037
Size*Aggregate	0.095
Size*Time	-0.361
Temperature	-0.681
Time	-0.400

The only parameter that has no significant correlation with creep stiffness is size. This indicates that there are no statistically significant differences between the creep stiffness functions of the 3x, 2x, and 1x beams. From Table 4, mixtures containing limestone are stiffer than mixtures with granite aggregate. This observation can be explained by the higher binder absorption of the limestone aggregate in comparison to the granite aggregate. Also, asphalt concrete prepared with unmodified asphalt binder has higher creep stiffness than asphalt concrete mixed with modified binder. Significant correlation is observed between the interaction term of

size and time and the creep stiffness: as time and size increases, the creep stiffness decreases. The correlation observed in the interaction terms is due to the highly statistical significance of the aggregate and time variables. As expected, significant correlation is observed between test temperature and creep stiffness.

The results of ANOVA are presented in Table 9. For a significance level of 5%, the variables with p -values smaller than 0.05 are significant and presented in bold.

Table 9. ANOVA for all temperatures

Variable	Estimate	Std. Error	t-value	p-value
Constant	3132.87	290.97	10.77	0
Size	-16.27	111.89	-0.15	0.884
Size*Aggregate	149.65	132.79	1.13	0.260
Size*Time	0.10	0.81	0.13	0.900
Binder[64-28]	1158.85	165.25	7.01	0
Binder[58-34]	288.82	240.86	1.20	0.231
Binder[64-34]	1934.80	249.58	7.75	0
Modified	-3601.87	165.05	-21.82	0
Aggregate	254.22	287.08	0.89	0.376
Temperature	-510.70	9.68	-52.75	0
Time	-19.73	1.74	-11.34	0

The parameters that are significant in the linear regression are: the factors from PG 64-34 and PG 64-28 binders, modification, temperature, and time. The positive coefficients for PG 64-34 and PG 64-28 indicate that mixtures prepared with these binders are stiffer than the mixtures prepared with PG 58-28. As indicated by the large t -values in Table 5, the variables that contain most of the information for the prediction of creep stiffness are modification, temperature, and time. As expected, when time and temperature increases, the creep stiffness of the mixture decreases.

The parameters in the regression that do not significantly contribute to the prediction of creep stiffness are size, aggregate type, and the interaction terms between size, aggregate and time. No significant difference is observed between the creep stiffness of mixtures prepared with PG 58-34 and with PG 58-28 (the reference level for binder PG in this analysis).

The results from this statistical analysis suggest that a representative creep stiffness of asphalt mixtures can be obtained from testing a minimum of three replicates of thin BBR asphalt mixture beams. Investigation of the microstructure of the thin beams, and finite element simulations of specimens of different sizes, not included in this summary, provided additional support to the feasibility of using BBR mixture beams to characterize asphalt mixtures.

Evaluate the Feasibility of Using Hirsch Model to Obtain Mixture Creep Stiffness from Binder Creep Stiffness

In this section, two models are investigated to obtain asphalt mixture properties from asphalt binder properties. The inverse problem is also analyzed since it can offer critical information related to the use of RAP in asphalt mixtures.

Hirsch Model

A semi-empirical model, based on Hirsch model (20), was proposed by Christensen et al. (21) to estimate the extensional and shear dynamic modulus of asphalt mixtures from asphalt binder experimental data. This approach would avoid the need for performing mixture experimental work, which is significantly more expensive than testing asphalt binders. The effective response is obtained by assembling the elements of the mixture in parallel and in series, as shown in Figure 36.

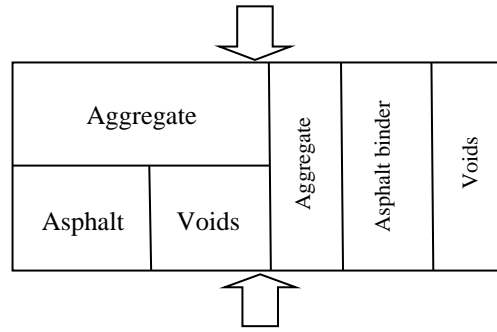


Figure 36. Semi-empirical Model Proposed by Christensen et al. (21)

The empirical factor P_c determines the amount of parallel or series elements in the mixtures. The general equation for this semi-empirical model is:

$$E_{mix} = P_c [E_{agg} V_{agg} + E_{binder} V_{binder}] + (1 - P_c) \left[\frac{V_{agg}}{E_{agg}} + \frac{(1 - V_{agg})^2}{E_{binder} V_{binder}} \right]^{-1} \quad [1]$$

where:

E_{mix} effective modulus of the mixture,
 E_{agg}, V_{agg} modulus and volume fraction of the aggregate,
 E_{binder}, V_{binder} modulus and volume fraction of binder, and
 P_c contact volume is an empirical factor defined as:

$$P_c = \frac{\left(P_0 + \frac{VFA \cdot E_{binder}}{VMA} \right)^{P_1}}{P_2 + \left(\frac{VFA \cdot E_{binder}}{VMA} \right)^{P_1}} \quad [2]$$

where:

VFA voids filled with asphalt binder (%),
VMA voids between mineral aggregate (%), and
P₀, P₁ and P₂ fitting parameters.

Zofka et al. (22) used the above model to predict BBR mixture stiffness from BBR extracted binder stiffness. The predicted values were always higher than the measured stiffness values, and as a consequence, the aggregate modulus, E_{agg} , was changed from 4,200,000 psi (29 GPa), to 2,750,000 psi (19 GPa) based on these results and on numerical manipulation. Further modification of the model was proposed by Zofka (16) who proposed a new expression for P_c :

$$P_c = 0.1 \ln \left(\frac{E_{binder}}{a} \right) + 0.609 \quad [3]$$

where:

E_{binder} effective modulus of the binder in GPa, and
 a constant equal to 1 GPa.

This modified model was used by Velasquez (17, 18) to estimate the asphalt mixture relaxation modulus calculated from BBR experimental data. It was found that the model predicted well the relaxation modulus of the majority of the mixtures investigated.

Analogical Models

The application of micromechanical models to asphalt materials characterization remains a very challenging task due to the complex structure of asphalt mixture and the complex interaction between the aggregate particles and the binder or mastic phase. A simpler approach may be more appropriate in this case, such as using analogical models.

Different analogical models are available in literature. Dashpot and springs constitute the simplest analogical linear viscoelastic models (23, 24). When spring and dashpot are assembled in series and in parallel, Maxwell and Kelvin-Voigt models can be constructed, respectively (Figure 37).

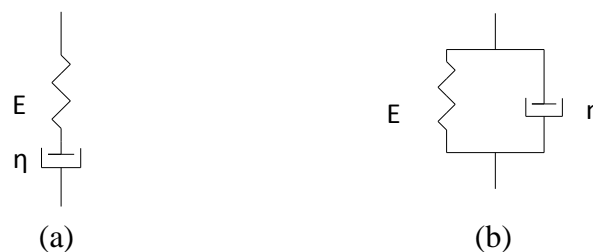


Figure 37. Maxwell Model (a) and Kelvin-Voigt Model (b)

These two models are not able to describe the complex properties of asphalt material but can be used as basic components of more sophisticated models. A satisfactory description of the behavior of asphalt binders and asphalt mixtures was obtained by Neifar and Di Benedetto (25) using a Generalized Maxwell Model and Generalized Kelvin-Voigt Model. Analogical models, with continuous rather than discrete spectra, were also applied to asphalt materials experimental data. The most important ones are presented next.

Huet Model

The Huet analogical model (26) is composed of two parabolic elements $J_1(t)=at^h$ and $J_2(t)=bt^k$ plus a spring (stiffness E_∞) combined in series. (Figure 38)

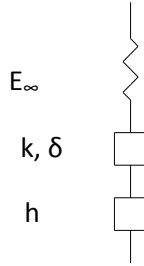


Figure 38. Huet Model

The Huet model was proposed for binders and mixtures and presents a continuous spectrum, which means it can be schematized by an infinite number of Kelvin-Voigt elements in series or Maxwell elements in parallel. The analytical expression of the Huet model for the creep compliance is:

$$D(t) = \frac{1}{E_\infty} \left(1 + \delta \frac{(t/\tau)^k}{\Gamma(k+1)} + \frac{(t/\tau)^h}{\Gamma(h+1)} \right) \quad [4]$$

where:

$D(t)$ creep compliance

E_∞ glassy modulus,

h, k exponents such that $0 < k < h < 1$,

δ dimensionless constant,

t time,

Γ gamma function that can be expressed as:

$$\Gamma(n) = \int_0^\infty t^{n-1} e^{-t} dt$$

$$\Gamma(n+1) = n\Gamma(n)$$

$n > 0$ or $\text{Re}(n) > 0$

t integration variable,

n argument of the gamma function.

τ characteristic time varying with temperature accounting for Time Temperature Superposition Principle (TTSP):

$$\tau = a_T(T) \tau_0(T_S)$$

a_T shift factor at temperature T that can be determined from Williams, Landel and Ferry (WLF) equation (27),

τ_0 characteristic time determined at reference temperature T_S .

An expression of the complex modulus for this model is also available; however, there is no analytical formula for the relaxation function:

$$E^*(i\omega\tau) = \frac{E_\infty}{1 + \delta(i\omega\tau)^{-k} + (i\omega\tau)^{-h}} \quad [5]$$

where:

i complex number ($i^2=-1$)
 E_∞ limit of the complex modulus for $\omega\tau \rightarrow \infty$ (Glassy modulus),
 ω 2π *frequency.

Huet-Sayegh Model

Huet model does not represent well mixture response at very low frequencies and high temperature, due to the inability to take into account the limiting value of the mixture modulus related to the aggregate skeleton. Sayegh (29) proposed a new expression for complex modulus introducing a spring in parallel in the Huet model (see Figure 39):

$$E^*(i\omega\tau) = E_0 + \frac{E_\infty - E_0}{1 + \delta(i\omega\tau)^{-k} + (i\omega\tau)^{-h}} \quad [6]$$

where:

i complex number ($i^2=-1$)
 E_∞ limit of the complex modulus for $\omega\tau \rightarrow \infty$ (Glassy modulus),
 E_0 limit of the complex modulus for $\omega\tau \rightarrow 0$,
 h, k exponents such that $0 < k < h < 1$,
 δ dimensionless constant,
 τ characteristic time varying with temperature accounting for the Time Temperature Superposition Principle (TTSP),
 ω 2π *frequency.

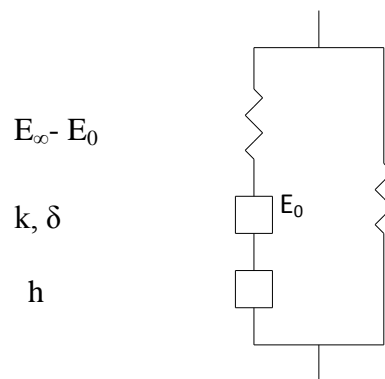


Figure 39. Huet-Sayegh Model (29)

Six constants are required in this model, δ , k , h , E_∞ , E_0 , and τ_0 , one more than the Huet model. The model was used by several authors (30, 31, 32, 33, 34, 35 and 36) with good results in the small strain domain for any range of frequencies and temperatures. It should be mentioned that this model has some limitation when predicting binder modulus at very low frequencies where,

instead of a parabolic element behavior, a linear dashpot would be more appropriate. The model was also used by Neifar (25) to calibrate a thermo-visco-plastic law named DBN law. This law allows describing with the same formalism different types of mixture behaviors according to the considered loading domain (37). A three dimensional extension of the DBN was also proposed by the same authors (38). It must be finally mentioned that there is no analytical expression for creep compliance in the time domain for this model.

2S2PID Model

An improved Huet-Sayegh model that takes into account the drawback for binder characterization was proposed by Di Benedetto & Olard (32, 39 and 40). This model is obtained from Huet-Sayegh model by adding a linear dashpot in series with the two parabolic elements and the spring of rigidity $E_\infty - E_0$ so that at low frequency it is equivalent to a linear dashpot in parallel with a spring of rigidity E_0 . The scheme of the model is shown in Figure 40 and the analytical expression of the complex modulus is given by [7].

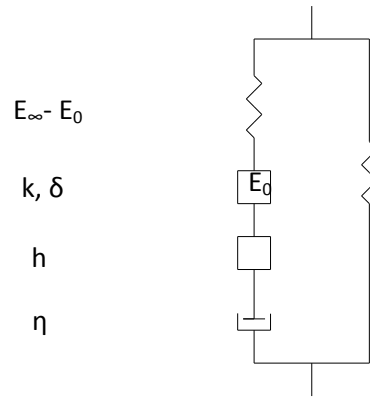


Figure 40. 2S2PID Model

$$E^*(i\omega\tau) = E_0 + \frac{E_\infty - E_0}{1 + \delta(i\omega\tau)^{-k} + (i\omega\tau)^{-h} + (i\omega\beta\tau)^{-1}} \quad [7]$$

where:

- i complex number ($i^2 = -1$)
- E_∞ limit of the complex modulus for $\omega\tau \rightarrow \infty$ (Glassy modulus),
- E_0 limit of the complex modulus for $\omega\tau \rightarrow 0$,
- h, k exponents such that $0 < k < h < 1$,
- δ dimensionless constant,
- β dimensionless parameter introduced to take into account the Newtonian viscosity of the linear dashpot
- τ characteristic time, varying with temperature, accounting for Time Temperature Superposition Principle (TTSP),
- ω 2π *frequency.

The seven constants (δ , β , k , h , E_∞ , E_0 , and τ) are determined from the experimental data at a reference temperature using an error minimization process.

ENTPE Transformation

Di Benedetto et al. (40) applied 2S2P1D model to experimental data obtained at a reference temperature $T_S=10^\circ\text{C}$ for a series of binders and corresponding mixtures. The authors found that the model parameters δ , k , h and β , respectively, were the same for the binder and the corresponding mixture, and only the static and glassy modulus, E_0 and E_∞ , and τ were different. The values of E_0 and E_∞ for the mixtures were in the range of 0.250 to 1.050GPa and 40 to 45GPa, respectively. From the simple regression of the mixture characteristic time, τ_{mix} , on the corresponding binder characteristic time, τ_{binder} , at the reference temperature on log scale, the authors found following relationship:

$$\tau_{\text{mix}}(T) = 10^\alpha \tau_{\text{binder}}(T) \quad [8]$$

where α is a regression coefficient depending on mixture and aging.

The value of α was determined in the range 2.66 to 2.82 according to the different mixtures and binders investigated.

Based on these findings, a relationship between the binder and the mixture complex moduli was proposed:

$$E_{\text{mix}}^*(\omega, T) = E_{0\text{mix}} + \left[E_{\text{binder}}^*(10^\alpha \omega, T) - E_{0\text{binder}} \right] \frac{E_{\infty\text{mix}} - E_{0\text{mix}}}{E_{\infty\text{binder}} - E_{0\text{binder}}} \quad [9a]$$

where:

E_{mix}^*	complex modulus of the mixture,
E_{binder}^*	complex modulus of the binder,
$E_{\infty\text{mix}}$	glassy modulus of the mixture,
$E_{0\text{mix}}$	static modulus of the mixture,
$E_{\infty\text{binder}}$	glassy modulus of the binder,
$E_{0\text{binder}}$	static modulus of the binder,
T	temperature,
ω	2π *frequency,
α	regression coefficient depending on mixture and aging.

The expression [9a] is independent of any rheological model and can be interpreted as a combination of three transformations (Figure 41):

- a negative translation of value E_{0_binder} along the real axis,
- a homothetic expansion starting from the origin with a ratio of $(E_{\infty_mix} - E_{0_mix}) / (E_{\infty_binder} - E_{0_binder})$,
- a positive translation of value E_{0_mix} along the real axis.

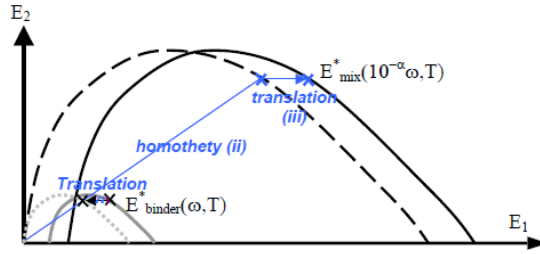


Figure 41. Binder to Mixture Transformation Scheme

Expression [9a] was also validated by Di Benedetto et al. (40) for mixtures and binders other than those used to derive the transformation. Delaporte et al. (41) used the same approach to investigate the linear viscoelastic properties of asphalt binder and mastics, with and without aging. Equation [9a] can be simply rearranged to obtain E^*_{binder} from $E^*_{mixture}$:

$$E^*_{binder}(\omega, T) = E_{0binder} + \left[E^*_{mix}(10^{-\alpha} \omega, T) - E_{0mix} \right] \frac{E_{\infty binder} - E_{0binder}}{E_{\infty mix} - E_{0mix}} \quad [9b]$$

Expressions [9a] and [9b] are called ENTPE (École Nationale des Travaux Publics de l'État) transformation.

Since the conversion of E^* to creep compliance is not trivial, it was decided to use Huet model that has an expression for creep compliance. This model does not present the additional dashpot in series and the spring in parallel that are present in the 2S2P1D model, which is acceptable since the experimental data of interest was obtained at low temperature. Validation of the ENTPE transformation that offers a simple relation between binder and mixture is also investigated for low temperature creep data.

Material and Testing

Materials used in the previous phase of the pooled fund study representing eight different asphalt binders and sixteen different asphalt mixtures prepared with the eight binders and with two types of aggregates (granite and limestone) were used in the experimental work. The binders were RTOFT aged and the mixtures were short term aged according to current AASHTO specifications. To avoid any errors associated with time-temperature superposition shifting, experimental data obtained at the same test temperature was considered for the binder-mixture analysis. Mixture testing was done with the BBR, following the procedure described in the previous section. Table 10 lists the eight binders, the sixteen corresponding mixtures investigated, and the test temperature considered. GR and LM stand for granite and for limestone, respectively. The volumetric properties of the mixtures are listed in Table 11, and the elastic modulus values for the two aggregates are listed in Table 12.

Table 10. Asphalt Binders and Mixtures

T(°C)	Binder	Mixtures	
		Granite (GR)	Limestone (LM)
-24	58-34:M1	58-34:M1:GR	58-34:M1:LM
-24	58-34:M2	58-34:M2:GR	58-34:M2:LM
-18	58-28:U1	58-28:U1:GR	58-28:U1:LM
-18	58-28:U2	58-28:U2:GR	58-28:U2:LM
-24	64-34:M1	64-34:M1:GR	64-34:M1:LM
-24	64-34:M2	64-34:M2:GR	64-34:M2:LM
-18	64-28:U1	64-28:U1:GR	64-28:U1:LM
-18	64-28:M1	64-28:M1:GR	64-28:M1:LM

Table 11. Mixture Volumetric Properties

	Granite mixtures	Limestone mixtures
Optimum asphalt content [%]	6.0	6.9
VMA [%]	16.3	16.2
VFA [%]	75.9	75.0

Table 12. Aggregate Modulus

Parameter	Granite	Limestone
Elastic modulus, $E_{elastic}$ [GPa]	30	25
([psi])	(4351131)	(3625942)

Data Analysis

Huet model expression in the time domain for the creep compliance is given by equation [4]. The expressions for binder and for mixture, respectively, can be written as follows:

$$D_{binder}(t) = \frac{1}{E_{\infty_binder}} \left(1 + \delta \frac{(t/\tau_{binder})^k}{\Gamma(k+1)} + \frac{(t/\tau_{binder})^h}{\Gamma(h+1)} \right) \quad [10]$$

$$D_{mix}(t) = \frac{1}{E_{\infty_mix}} \left(1 + \delta \frac{(t/\tau_{mix})^k}{\Gamma(k+1)} + \frac{(t/\tau_{mix})^h}{\Gamma(h+1)} \right) \quad [11]$$

where

$D_{binder}(t), D_{mix}(t)$ creep compliance of binder and mixture,
 $E_{\infty_binder}, E_{\infty_mix}$ glassy modulus of binder and mixture,
 $\tau_{binder}, \tau_{mix}$ characteristic time of binder and mixture.

The five constants required by the model, δ , k , h , E_{∞} , and τ , were determined through minimization of the sum of the distances between the experimental creep compliance and that Huet model at n time points:

$$\min \left(\sum_{i=1}^n [D^{\text{exp}}(t) - D^{\text{Huet}}(t)]^2 \right) \quad [12]$$

where:

$D^{\text{exp}}(t)$ experimental creep compliance,
 $D^{\text{Huet}}(t)$ model creep compliance.

Figures 42 and 43 provide examples on how the model fits the experimental data for PG 58-34 M2 modified asphalt binder and the corresponding asphalt mixture made with granite aggregate and tested at $T=-24^{\circ}\text{C}$, and for PG 58-28U2 plain asphalt binder and the corresponding limestone asphalt mixture tested at $T=-18^{\circ}\text{C}$, respectively.

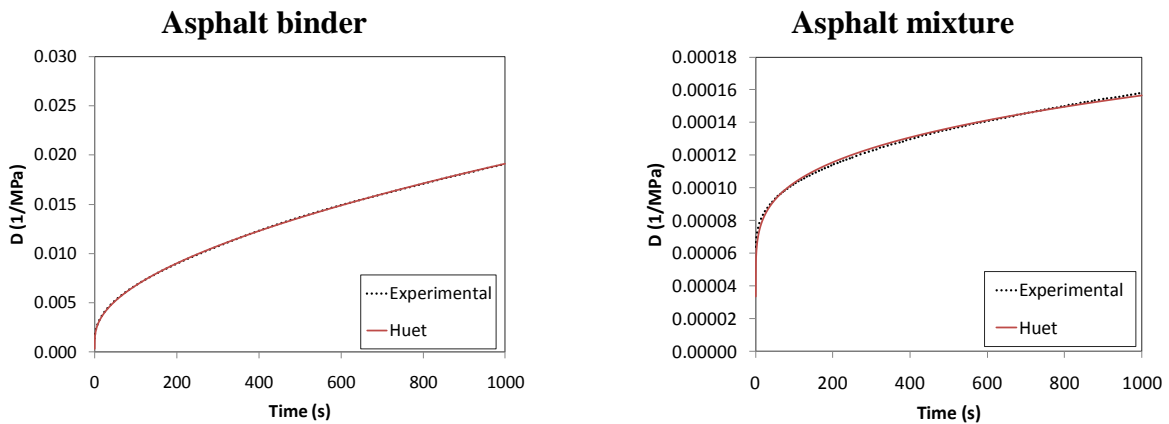


Figure 42. Huet Model for PG 58-34 M2 Binder and Granite mixture, $T=-24^{\circ}\text{C}$

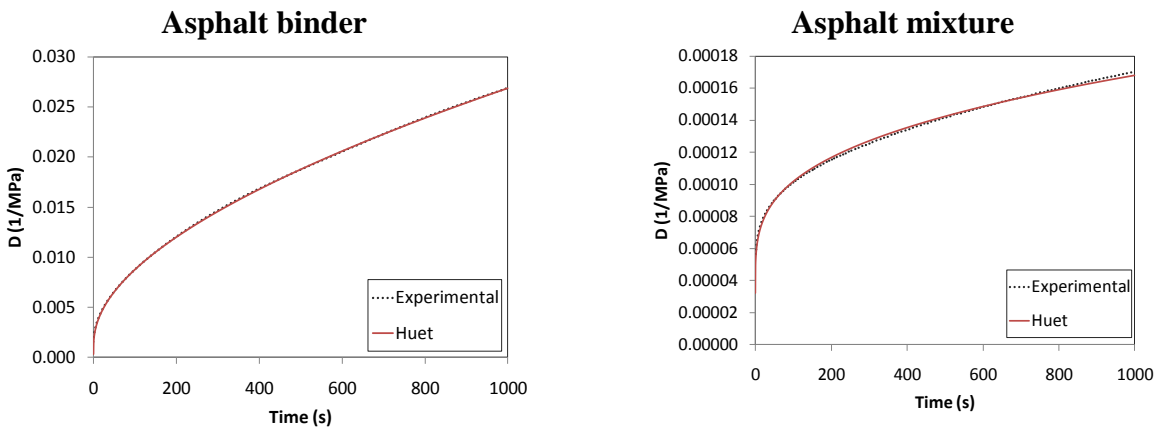


Figure 43. Huet Model for PG 58-34 M2 Binder and Limestone Mixture, $T=-24^{\circ}\text{C}$

Visual inspection indicates that Huet model fits asphalt binder and mixture experimental data very well. This is true for all binders and all mixtures evaluated. Table 13 lists the parameters of

the model for four of the asphalt binders and the corresponding granite mixtures made with the same mix design and tested at $T=-24^{\circ}\text{C}$.

Table 13. Huet Model Parameters for Binders and Granite Mixtures

Material		δ	k	h	E_{∞} (MPa)	$\text{Log}(\tau)$
Binder	58-34:M1	2.42	0.18	0.60	3000	0.251
	58-34:M2	4.18	0.22	0.62	3000	0.497
	64-34:M1	3.50	0.21	0.64	3000	0.387
	64-34:M2	3.99	0.23	0.64	3000	0.328
Mixtures	58-34:M1:GR	2.42	0.18	0.60	28000	3.420
	58-34:M2:GR	4.18	0.22	0.62	30000	3.675
	64-34:M1:GR	3.50	0.21	0.64	30000	3.547
	64-34:M2:GR	3.99	0.23	0.64	29001	3.523

It is observed that the values for δ , k, and h are the same for the binder and the corresponding mixture. It is also observed that the binders have similar values of δ , k, and h, identical glassy modulus E_{∞} (3000 MPa), and different characteristic time τ . The same is true for the mixtures; in this case glassy modulus is in the 28000-30000 MPa range. The values of the characteristic time of mixtures were compared with those found by Huet (26) and reasonable agreement was found.

In addition, by plotting $\log(\tau_{\text{binder}})$ vs. $\log(\tau_{\text{mix}})$, a linear correlation can be detected. Figures 44 and 45 contain the characteristic time plots for all binders and their corresponding granite and limestone mixtures at the reference temperatures ($T=24^{\circ}\text{C}$ for PG-34 and $T=18^{\circ}\text{C}$ for PG-28).

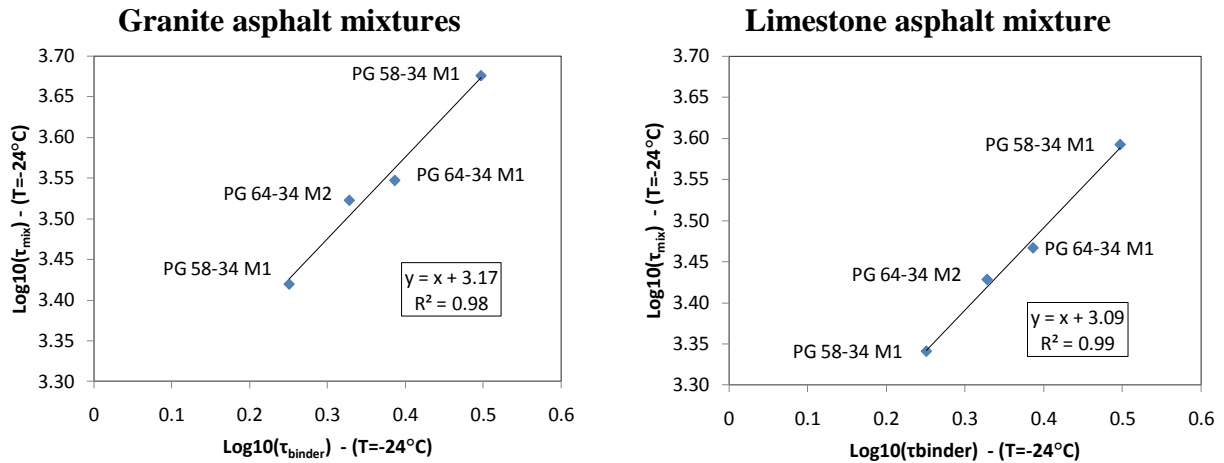


Figure 44. Characteristic Time Relationship for PG-34 Binders and Corresponding Mixtures

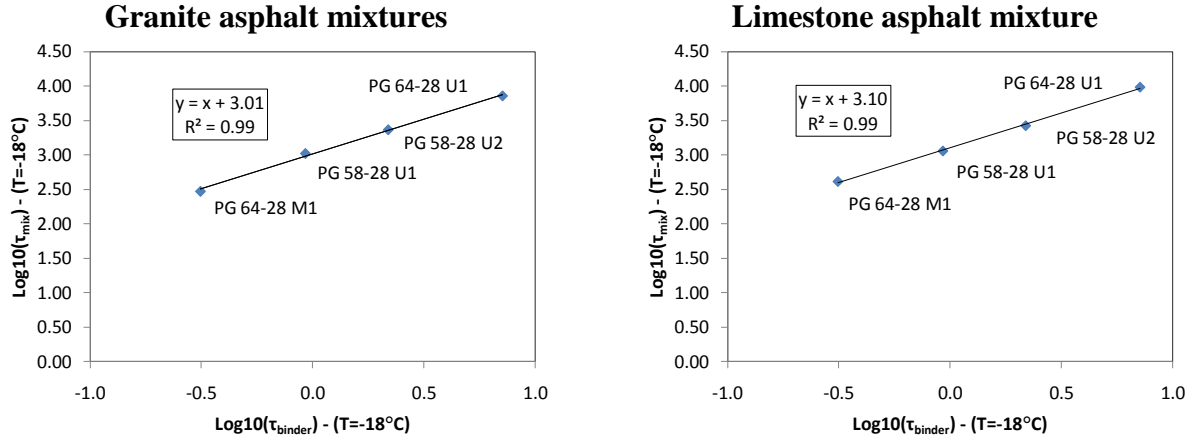


Figure 45. Characteristic Time Relationship for PG-28 Binders and Corresponding Mixtures

Based on the strong linear correlation ($R^2=0.98-0.99$), the following expression can be written to relate the characteristic time of the binders and of the corresponding mixtures with similar mix designs:

$$\tau_{mix} = 10^{\alpha} \tau_{binder} \quad [13]$$

where:

- τ_{binder} characteristic time of binder,
- τ_{mix} characteristic time of mixture,
- α regression parameter which may depend on mix design.

Table 14 lists the α values for all materials.

Table 14. α Values for the Four Binders Mixtures Groups				
Mixtures	PG -34 granite	PG -34 limestone	PG -28 granite	PG -28 Limestone
α	3.17	3.09	3.01	3.10
Difference	0.08		0.09	

The α values are very similar and range from 3.01 to 3.17, which reflects the fact that the mix designs were very similar even though the mixtures contain different type of aggregates. These values are also similar to the results reported by Olard and Di Benedetto for 2S2P1D model (32, 39, 40).

Combining [10], [11] and [13] the following expression can be written:

$$D_{mix}(t) = D_{binder}(t10^{-\alpha}) \frac{E_{\infty_binder}}{E_{\infty_mix}} \quad [14]$$

which can be also written in terms of the inverse of creep compliance, creep stiffness $S(t)$:

$$S_{mix}(t) = S_{binder}(t10^{-\alpha}) \frac{E_{\infty_mix}}{E_{\infty_binder}} \quad [15a]$$

This expression can be simply rearranged to express S_{binder} as a function of S_{mix} as follows:

$$S_{binder}(t) = S_{mix}(t10^{\alpha}) \frac{E_{\infty_binder}}{E_{\infty_mix}} \quad [15b]$$

where:

$D_{mix}(t)$	creep compliance of mixture,
$D_{binder}(t)$	creep compliance of binder,
$S_{mix}(t)$	creep stiffness of mixture,
$S_{binder}(t)$	creep stiffness of binder,
E_{∞_mix}	glassy modulus of mixture,
E_{∞_binder}	glassy modulus of binder,
α	regression parameter which may depend on mix design,
t	time

These expressions are similar to expressions [9a] and [9b] and represent the ENTPE transformation for low temperature creep stiffness. They were used next to solve the forward and the inverse problem.

Forward Problem: mixtures from binders

Two approaches were used: Hirsch model and ENTPE transformation. For Hirsch model, equations [1], [2], and [3], were applied to the experimental data. Two formulations of the Hirsch model were used according to results obtained in previous work (16, 17, 18, 22, 42). In one study (22), a value of aggregate modulus different from the original formulation proposed by Christensen (21) was used ($E_{agg}=2750000\text{psi} - 19\text{GPa}$ instead of $E_{agg}=4200000\text{psi} - 29\text{GPa}$) with better fitting results. The alternative formulation of the P_c contact volume parameter [3] was applied in other studies (16, 17, 18 and 42) in which the aggregate modulus was set to 25GPa and 30GPa for limestone and granite respectively. Table 7 summarizes the parameters used for the models evaluation; G stands for granite and L for limestone.

Table 15. Parameters Used in Hirsch Model

Granite	Limestone
Hirsch-2	Hirsch-2
$E_a=2750000\text{psi}$	$E_a=2750000\text{psi}$
P_c expression [2]	P_c expression [2]
Hirsch-3G	Hirsch-3L
$E_a=4351131\text{psi}$	$E_a=3625942\text{psi}$
P_c expression [3]	P_c expression [3]

Figures 46 to 49 contain plots of experimental data and creep stiffness predictions for granite and limestone mixtures.

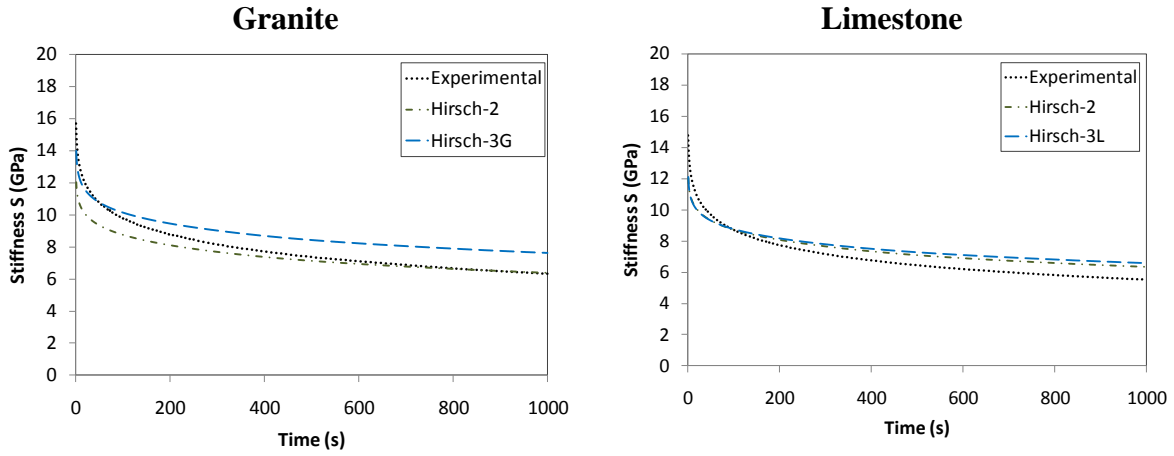


Figure 46. Hirsch Model Predictions for PG 58-34 M2Mixture, T=-24°C

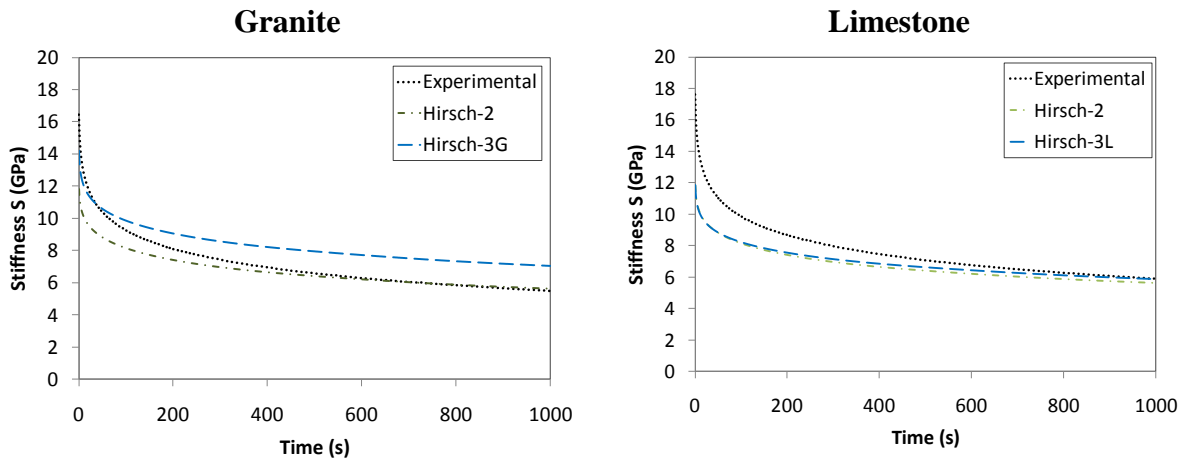


Figure 47. Hirsch Model Predictions for PG 58-28 U2 Mixtures, T=-18°C

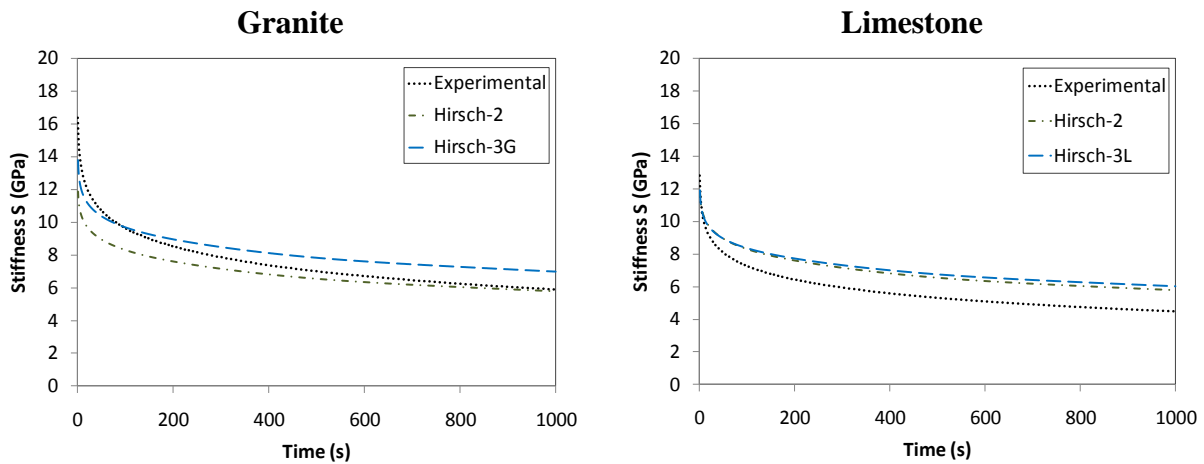


Figure 48. Hirsch Model Predictions for PG 64-34 M2Mixture, T=-24°C

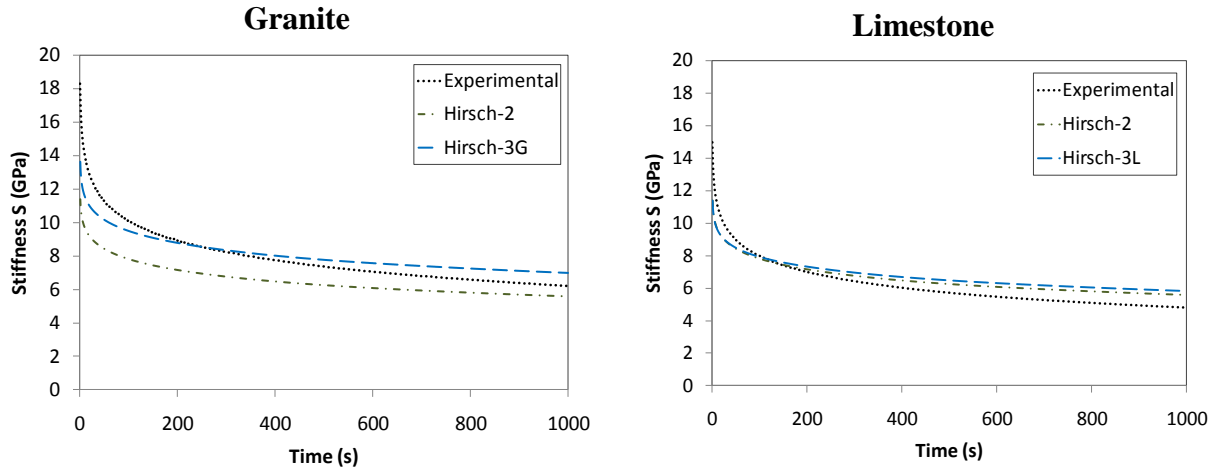


Figure 49. Hirsch Model Predictions for PG 64-28 M1 Mixtures, T=-18°C

For the granite mixtures, the experimental curves are located between the two prediction curves: Hirsch-2 and Hirsch-3G. Different conclusions can be drawn for the limestone mixtures: Hirsch-2 and Hirsch-3L result in similar prediction curves and both overestimate the experimental data except for the limestone mixture PG 58-28 U2 tested at T=18°C. Overall, the Hirsch model seems to reasonably predict the creep stiffness of most mixtures investigated.

For the ENTPE transformation, equation [15a] was used to solve the forward problem for the asphalt binders and mixtures investigated. Figures 50 to 53 contain plots of the experimental data and transformation predictions for granite and limestone mixtures at T=-24°C and T=-18°C.

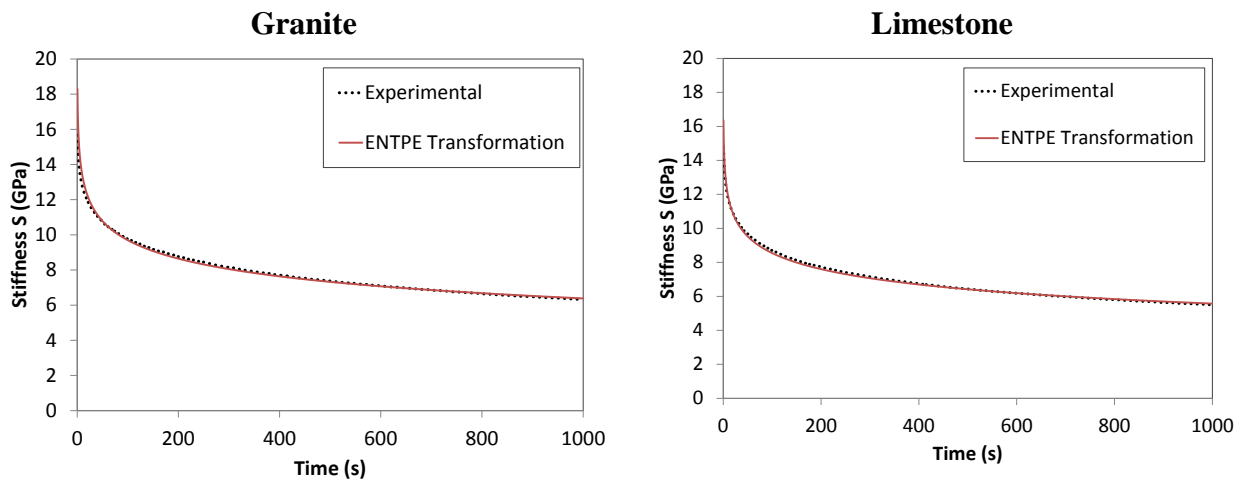


Figure 50. ENTPE Transformation for PG 58-34 M2 Mixtures, T=-24°C

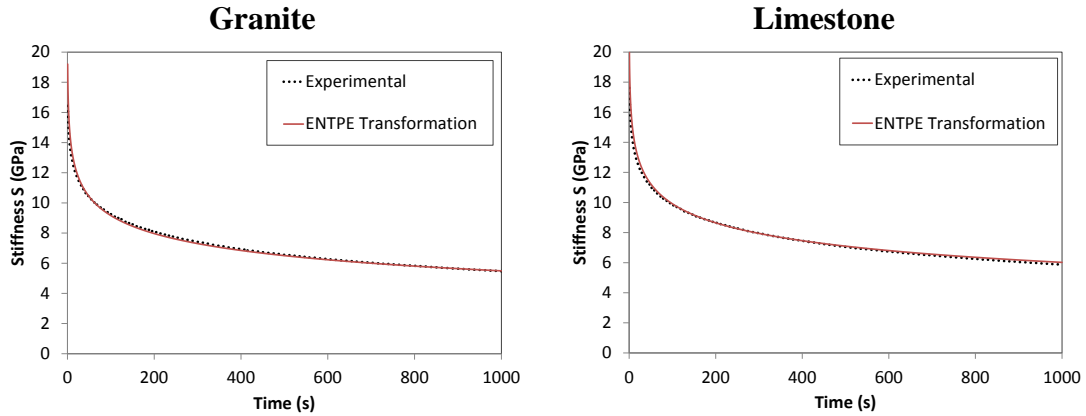


Figure 51. ENTPE Transformation for PG 58-28 U2 Mixtures, T=-18°C

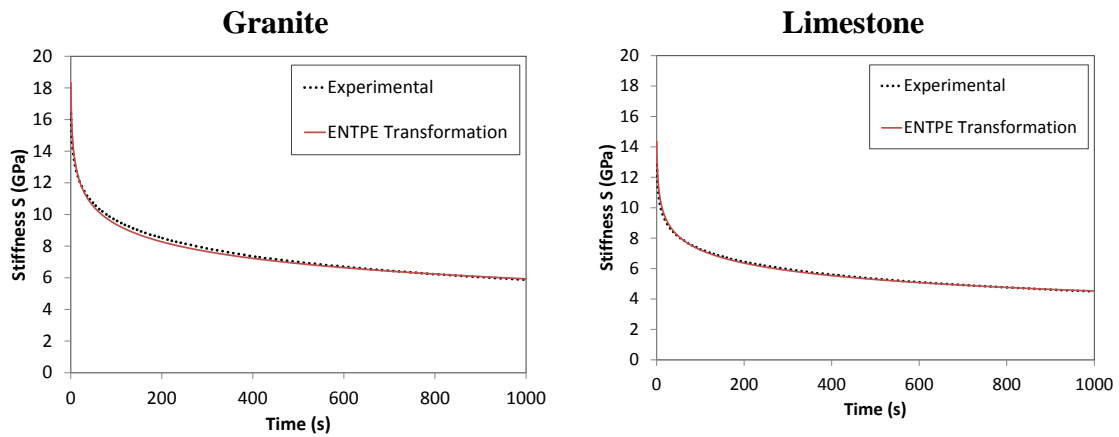


Figure 52. ENTPE Transformation for PG 64-34 M2 Mixture, T=-24°C

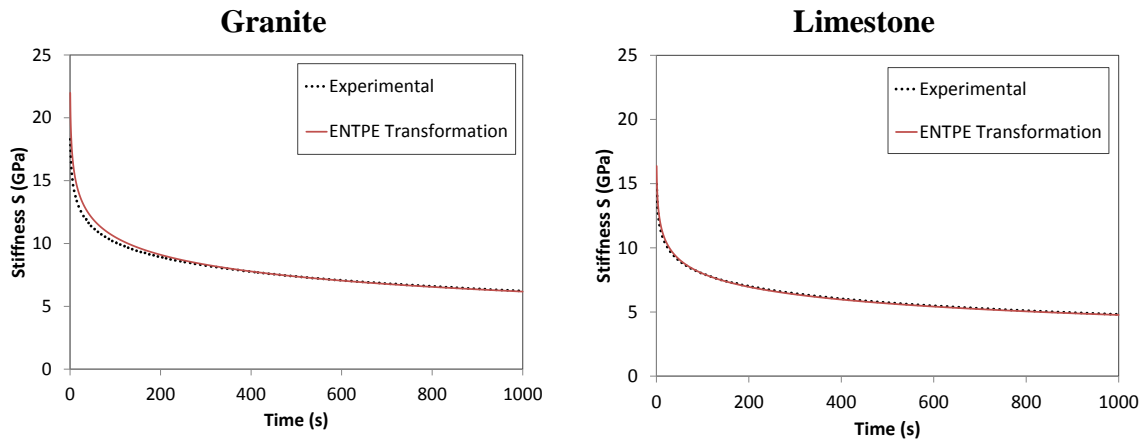


Figure 53. ENTPE Transformation for PG 64-28 M1 Mixtures, T=-18°C

The transformation fits very well the experimental creep stiffness $S(t)$ for all mixtures investigated and appears to predict the creep behavior of asphalt mixtures at low temperatures using asphalt binder data better than Hirsch model.

Inverse Problem: Binders from Mixtures

The prediction of a material property based on the measured (or observed) material response constitutes the objective of an inverse problem in mechanics. This process is called a parameter identification procedure. Two procedures for parameter identification for viscoelastic materials were proposed by Ohkami and Swoboda (43). Both methods contain boundary control concept introduced by Ichikawa and Ohkami (44). Amin et al (45) developed a similar approach by combining FEM simulations with inverse scheme. The viscoelastic behavior was modeled by the authors using a 3-parameter solid model. Kim and Kreider (46) used numerical inversion for 2D problem for linear viscoelastic homogenous material with three-seven parameters. Several potential problems with this scheme were detected. The solution might not be unique and might depend on the initial guess for optimization method and moreover there is no unique optimization approach that is suitable for all problem and material types.

Zofka et al. (22) used modified Hirsch (20) model proposed by Christensen (21) to “back-calculate” the asphalt binder stiffness and m-value from mixture creep stiffness at low temperatures. Since brute force was time consuming, the original equation [1] was combined with an alternative procedure to the numerical minimization based on the observation that a simple function could be fitted to the mix creep stiffness versus binder creep stiffness data. Based on these findings, Velasquez et al. (3) using additional experimental data developed two expressions for the Pc parameter [14] and [15]. Zofka (16) also used an inverse scheme based on the Zevin’s method of iterative functions (47). The asphalt mixture is treated as a 2-phase composite material consisting of elastic aggregate particles of arbitrary shape and viscoelastic asphalt mastic.

Hirsch Model

The method proposed by Zofka et al. (22) was used. First, based on the volumetric properties of the mixtures, plots of binder creep stiffness versus predicted mixture stiffness using modified equation [1] are generated for binder stiffness values between 50 to 1000MPa (Figures 20 and 21). Then, a very simple function is fitted to the mix log stiffness versus binder log stiffness data, as shown in Figure 54 and 55:

$$E_{mix} = a \cdot \ln(E_{binder}) + b \quad [16]$$

where a and b are regression parameters.

Finally, the binder stiffness is simply calculated using equation [16] over the entire range of loading time.

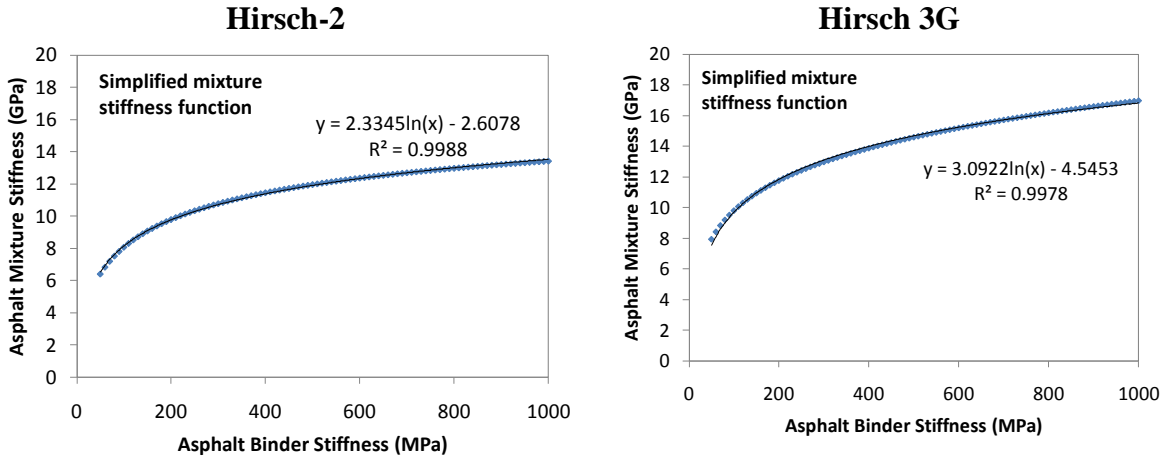


Figure 54. Simplified Mixture Function for Granite Mixture

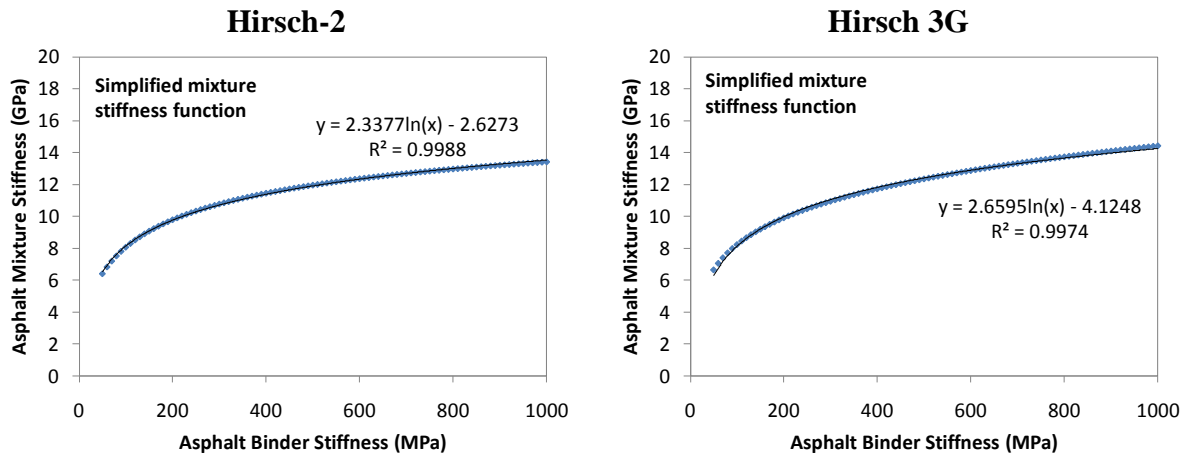


Figure 55. Simplified Mixture Function for Limestone Mixture

The parameters in Table 15 were introduced in the back calculation process along with the volumetric properties of the sixteen mixtures investigated. The back calculation algorithm was applied to the mixture data and binder creep stiffness was predicted and compared to the creep stiffness experimentally determined for the RTFOT binders used to prepare the corresponding mixtures. Figures 56 to 59 present examples for four of the binders investigated.

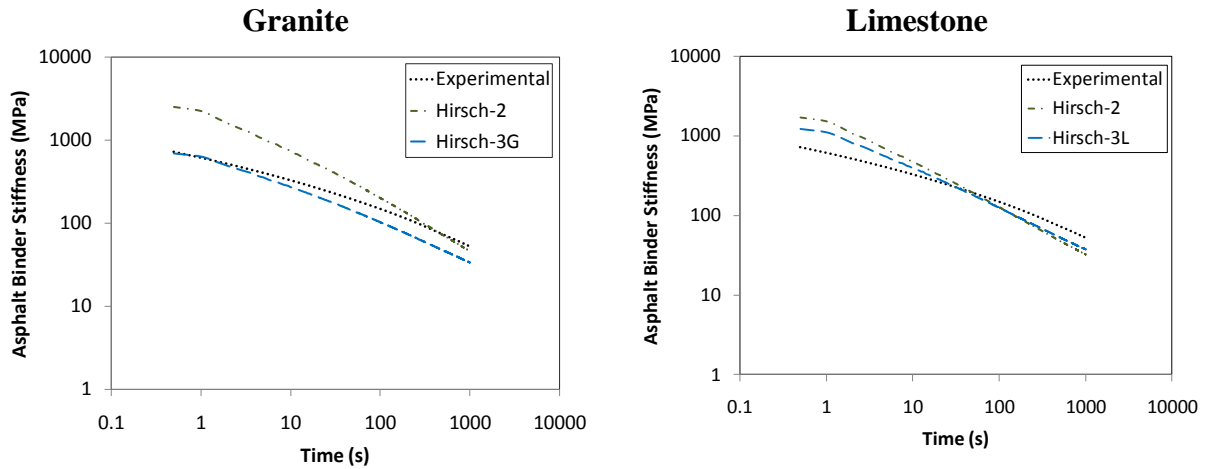


Figure 56. Predicted (Hirsch) Binder Creep Stiffness for PG 58-34 M2 Mixtures, T=-24°C

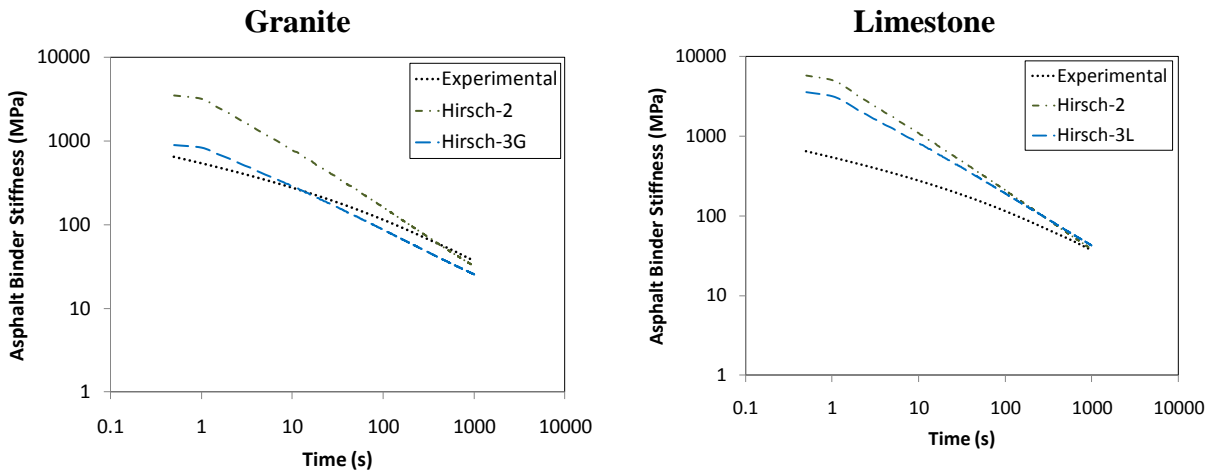


Figure 57. Predicted (Hirsch) Binder Creep Stiffness for PG 58-28 U2 Mixtures, T=-18°C

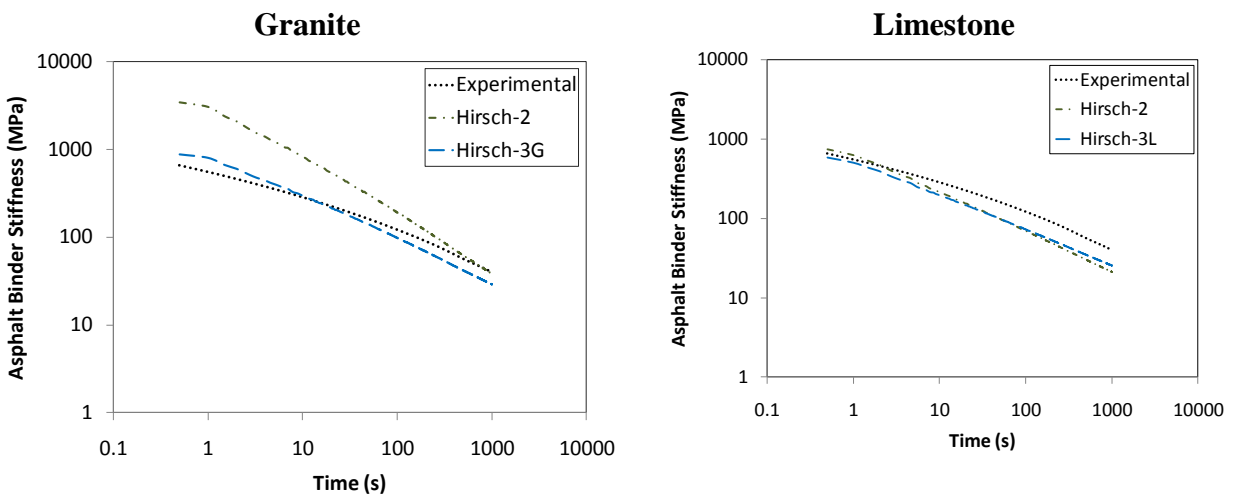


Figure 58. Predicted (Hirsch) Binder Creep Stiffness for PG 64-34 M2 Mixtures, T=-24°C

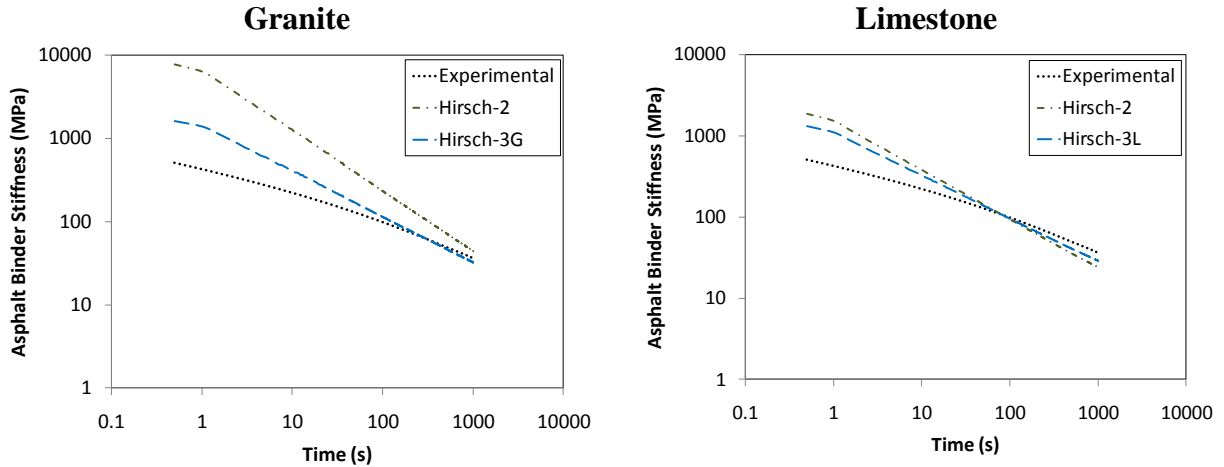


Figure 59. Predicted (Hirsch) Binder Creep Stiffness for PG 64-28 M1 Mixtures, T=-18°C

For granite and limestone mixtures, the back calculated binder stiffness fit the experimentally determined binder creep stiffness poorly with a few exceptions.

ENTPE Transformation

In this case, the approach is straight forward. First, from equation [13] the binder characteristic time is obtained from mixture characteristic time:

$$\tau_{binder} = 10^{-\alpha} \tau_{mix} \quad [17]$$

Then, asphalt binder creep stiffness S_{binder} can be easily predicted from asphalt mixture creep stiffness S_{mix} using equation [15b]. Figures 60 to 63 contain plots of predicted binder creep stiffness $S(t)$ obtained using equation [15b] for granite and limestone mixtures at T =-24°C and T=-18°C.

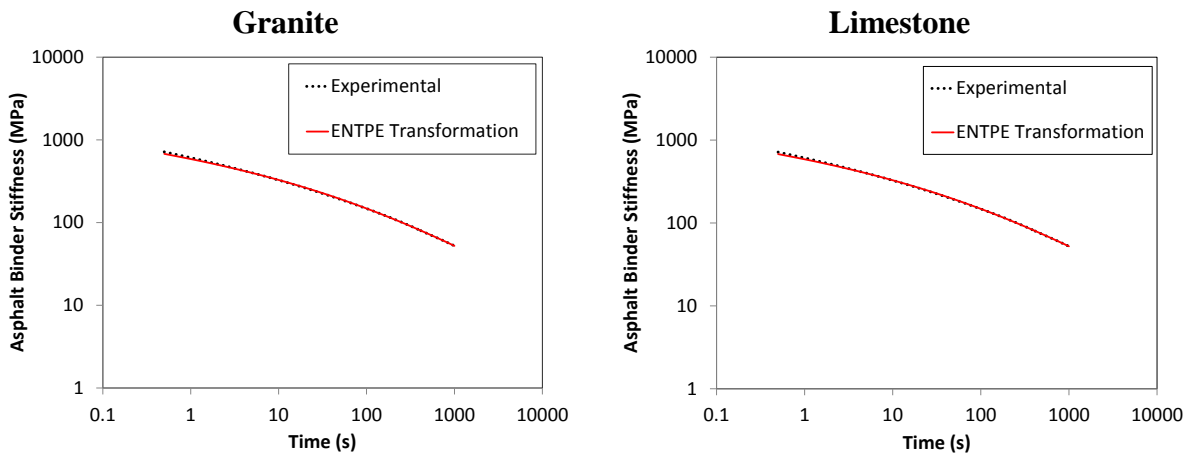


Figure 60. ENTPE Transformation for PG 58-34 M2 Mixtures, T=-24°C

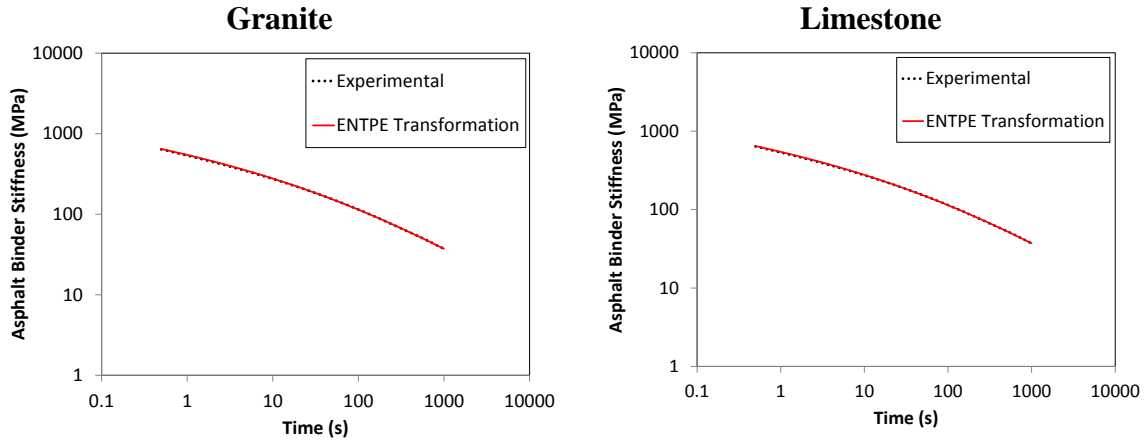


Figure 61. ENTPE Transformation for PG 58-28 U2 Mixtures, T=-18°C

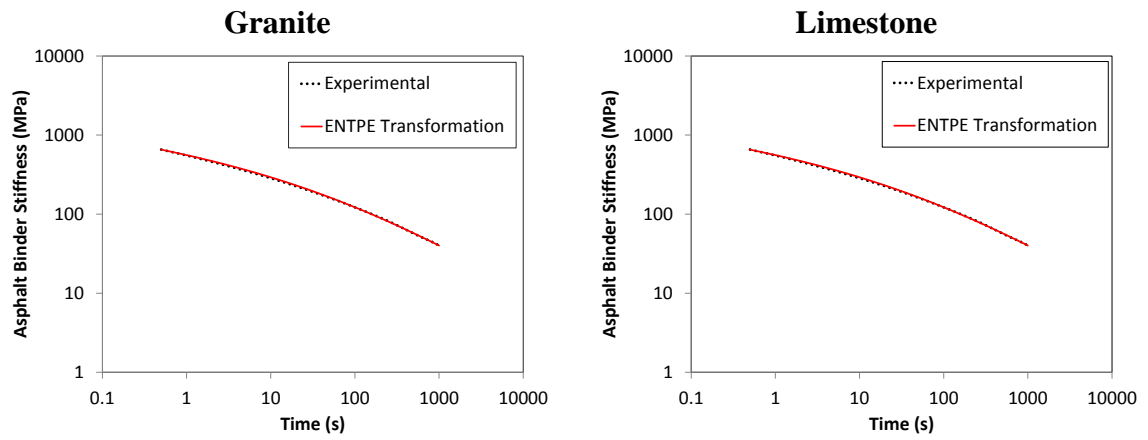


Figure 62. ENTPE Transformation for PG 64-34 M2 Mixtures, T=-24°C

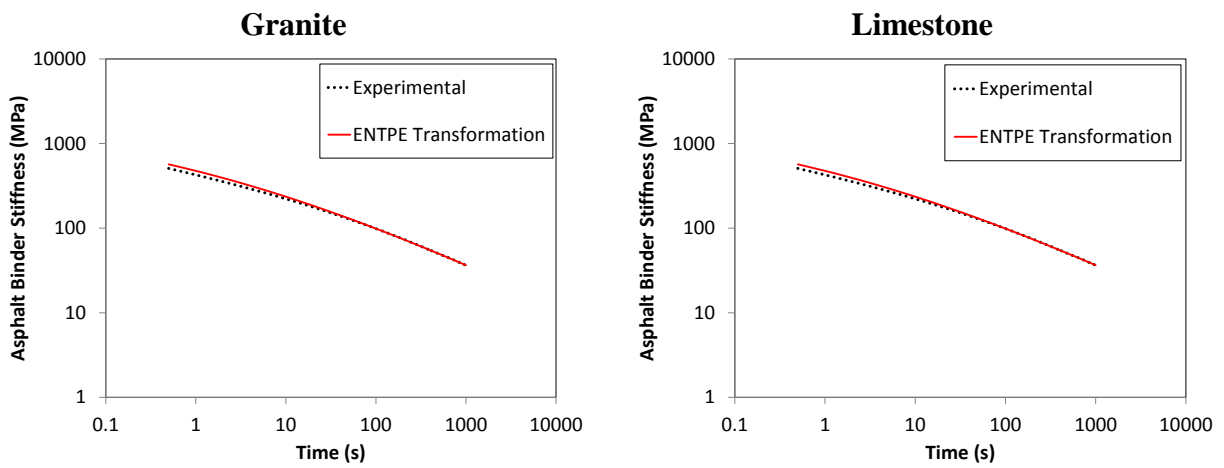


Figure 63. ENTPE Transformation for PG 64-28 M1 Mixtures, T=-18°C

It is obvious that expression [15b] predicts asphalt binder creep stiffness very well for all mixtures investigated.

Conclusions

Based on the results, the following conclusions are drawn:

- Hirsch model predicted reasonably well the creep stiffness of the majority of mixtures investigated using binder creep stiffness and volumetric information. There was a small tendency to over predict the stiffness for the limestone mixtures.
- For inverse problem, Hirsch model prediction of asphalt binder creep stiffness from asphalt mixture creep stiffness was poor. This may be due to the simplification used to fit the model expression.
- ENTPE transformation performed very well for both forward and inverse problems. In particular, for the inverse problem of numerically “extracting” asphalt binder creep stiffness from experimental mixture data, the transformation performed much better than Hirsch model. However, the main obstacle is obtaining a reasonably accurate value for α parameter.

Using Binder Creep Stiffness to Obtain Mixture Creep Stiffness Threshold Value

As mentioned in subtask 2, the development of the SHRP asphalt binder criterion for low temperature cracking was based on the assumption that the 2-hour mixture stiffness correlated well with the severity of thermal cracking in the field (1). This assumption was extended to asphalt binder stiffness obtained in low-temperature creep tests. N. W. McLeod tentatively concluded that the critical low temperature pavement modulus of stiffness at which transverse pavement cracking is likely to occur is 1,000,000 psi or 7GPa. A value twice as high was proposed by Redshaw.

The research performed in the previous section demonstrated that mixture creep stiffness can be predicted using binder creep stiffness data. One interesting application is to predict what is the mixture creep stiffness value corresponding to a binder creep stiffness value of 300MPa, the current PG specification limit. The challenge is to reasonably match the aging condition of the two materials. Since it is generally accepted that binder RTFOT matches the aging condition of the mixture after short term aging or as loose mix, it was decided to first determine the corresponding creep stiffness limit for binders in RTFOT condition and then use Hirsch model to predict mixture creep stiffness. The asphalt binders used in the first phase of the pooled fund study (see Table 10) were also used here because BBR data was obtained for both PAV and RTFOT conditions.

Binder PAV to Binder RTFOT

First, the BBR binder PAV data was used to calculate the critical temperature at which $S(60s)$ is equal to 300MPa. This was done by assuming a linear relation between $\log S(60s)$ and test temperature and interpolating to obtain the critical temperature, as shown in Figure 64a. Then, based on the same linearity assumption between the RTFOT $\log S(60s)$ and temperature, a corresponding stiffness value at the critical temperature is obtained, as shown in Figure 64b

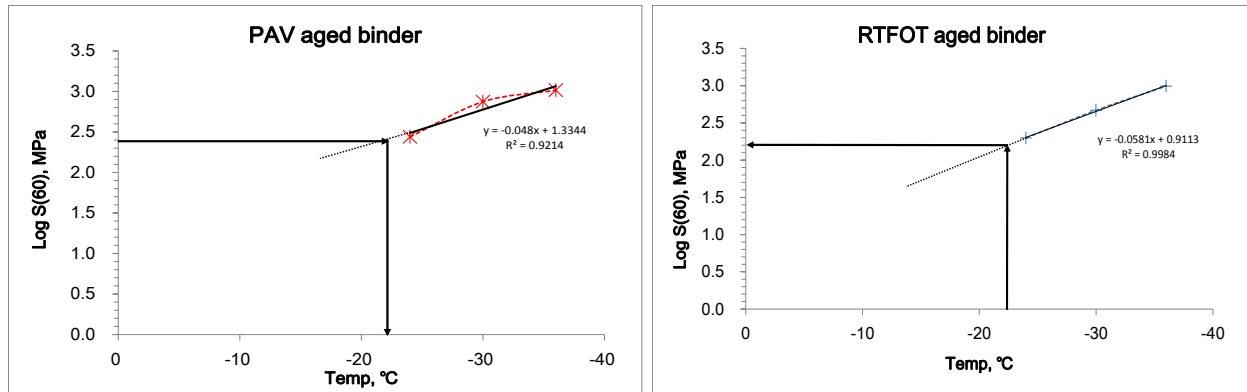


Figure 64. Predicting $S(60)_{RTFOT}$ corresponding to $S(60)_{PAV} = 300\text{MPa}$

Since log creep stiffness for some of the binders did not follow a linear relation to temperature, another approach based on the CAM model was used. In this case, creep stiffness master curves were obtained using the model expression for stiffness:

$$S(t) = S(t)_g \cdot \left[1 + \left(\frac{t_c}{t} \right)^v \right]^{-w/v} \quad [18]$$

Where, $S(t)_g$: glassy creep stiffness asymptote (3GPa);

t_c : cross over time, v and w : fitting parameters

Table 16 summarizes the results of the two methods. No significant differences are observed between the simple regression method and CAM model fitting except for two binders.

Table 16. Binder PAV T_{cr} and Corresponding $S(60)_{RTFOT}$

Mix ID	PG Binder Grade	T_{cr} [PAV]	Simple Regression			CAM	Error [%]
			$S(60s)_{T_{cr}}$ [MPa]	R^2 [PAV]	R^2 [RTFOT]	$S(60s)_{T_{cr}}$ [MPa]	
B	58-34 M1	23.8	196	0.921	0.998	192	2.3
C	58-34 M2	26.5	255	0.992	0.994	289	11.6
D	58-28 U1	23.5	229	*	0.995	221	3.4
E	58-28 U2	20.5	180	0.996	*	178	0.9
F	64-34 M1	24.5	197	0.985	0.986	189	4.5
G	64-34 M2	27.0	238	0.985	0.994	294	19.0
H	64-28 U1	20.0	258	0.999	*	247	4.6
I	64-28 M1	23.7	261	0.999	0.999	263	0.9
J	64-22 U1	18.4	124	*	*	123	1.1

*: only two temperatures were considered.

Binder RTFOT to Mixture

Asphalt mixture creep stiffness was predicted from RTFOT binder creep stiffness by means of Hirsch model previously described. Table 17 and Figure 65 summarize the results.

Table 17. Predicted Mixture S(60) at PAV Binder Critical Temperature

Mix ID	S(60s) _{Tcr} [MPa]	Mix ID	S(60s) _{Tcr} [MPa]
B: G	10864	B: L	10873
C: G	12146	C: L	12156
D: G	11310	D: L	11319
E: G	10644	E: L	10654
F: G	10814	F: L	10823
G: G	12204	G: L	12214
H: G	11647	H: L	11657
I: G	11854	I: L	11864
J: G	9521	J: L	9530

*: G: Granite, L: Limestone

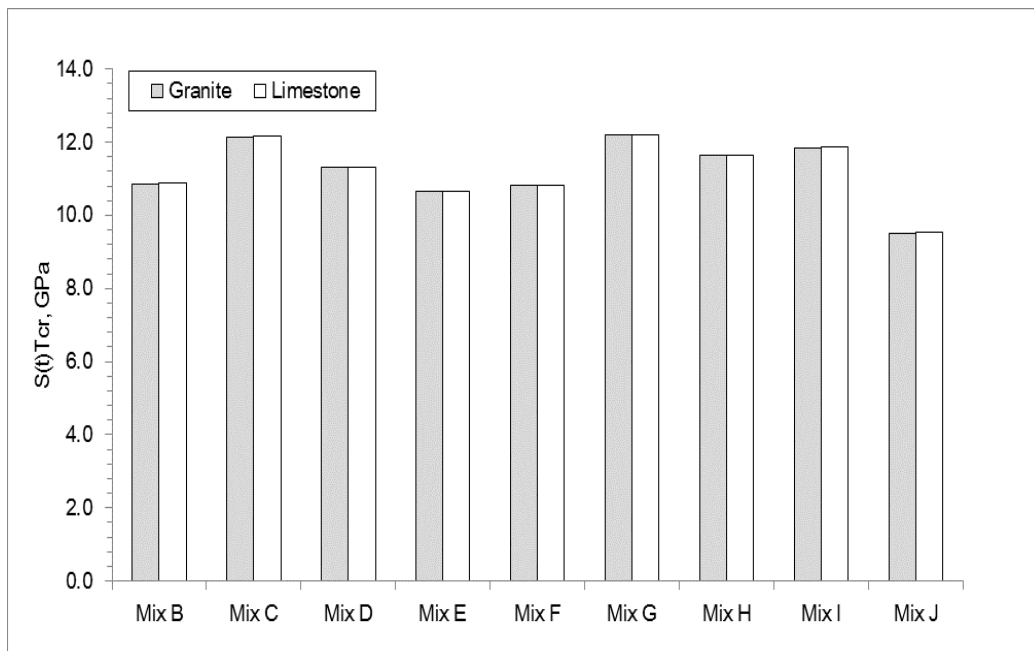


Figure 65. Predicted Mixture S(60) at PAV Binder Critical Temperature

It can be observed that the values range from 9.5GPa to approximately 12GPa. Since they represent the short term aging condition of the mixtures, it is expected that higher values would be obtained for long term aged mixtures, closer to the limit proposed by Redshaw.

Obtaining Strength from BBR Tests on Mixture Beams

As already mentioned, research performed at the University of Minnesota showed that the Bending Beam Rheometer (BBR), currently used for asphalt binders specifications, can be used to obtain creep properties of asphalt mixtures, see Figure 31.

Work performed in an ongoing NCHRP Idea project investigates the feasibility of using BBR to obtain asphalt mixture bending strength. A summary of the results is presented in the next paragraphs.

Experimental Work

The TE-BBR Pro device provided by Canon Instrument Company was used to perform the strength tests. The new machine, shown in Figure 66, is equipped with a proportional valve that offers a much more complex control of the pressure in the air bearing system and is capable of providing constant loading rates to perform strength tests. The new load cell capacity is 44N.



Figure 66. TE-BBR Pro device

Three asphalt binders used in phase I of the pooled fund study, for which DTT results were available, were investigated: PG 58-28 (unmodified), PG 58-34 (SBS modified) and PG 64-22 (unmodified). The first two asphalt binders were short and then long termed aged and bending strength tests were performed using the new BBR device for both aging conditions. DTT strength results were available for both aging conditions at which BBR strength tests were run. Binder PG 64-22 was used in the second part of the experimental phase, in which BBR strength tests were run in ethanol and in potassium acetate. All tests results for this asphalt binder were obtained for RTFOT condition.

The loading procedure for the first two asphalt binder was selected such that DTT and BBR times to failure for PAV aged binder tested at lower PG+10°C were similar. This approach was selected based on the fact that the cohesive law, governing the fracture process zone (FPZ) propagation, is rate dependent and consequently time dependent. By selecting similar times to failure for the two tests, the FPZ propagation is imposed to occur with the same rate. This was done to obtain a procedure that facilitates the comparison of DTT and BBR strength since the two tests are performed using different loading procedures: displacement and load control, respectively.

The BBR nominal strength (maximum stress at peak load) σ_N and corresponding strain ϵ_N at the bottom of the thin beam (Figure 67a) can be estimated from the dimensions of the beam, the applied load, and the measurement of deflection.

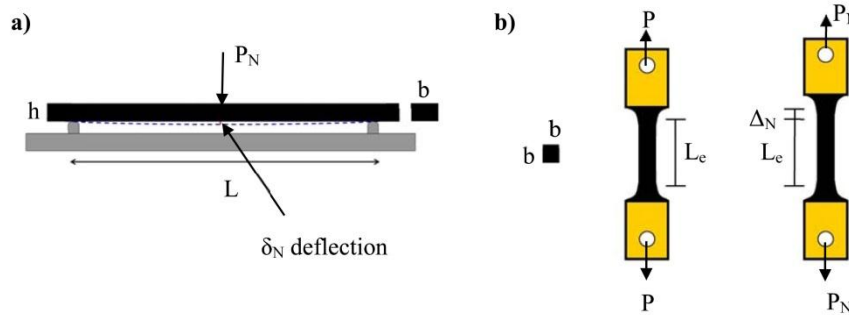


Figure 67. BBR (a) and DTT (b) strength tests

Table 18 summarizes the results obtained from BBR strength tests for the first two binders and Table 19 the results from DTT strength tests.

Table 18. BBR asphalt binder test results

Binder PG	Aging	Temperature (°C)	Rate N/min	Mean Strength (MPa)	CV (%)
58-28	RTFO	-18	1.4	1.4	39.9
			5.6	1.8	22.4
		-24	1.4	1.6	13.2
	5.6		1.6	20.3	
	PAV	-18	1.4	1.9	23.7
			5.6	2.1	17.1
-24		1.4	1.8	42.6	
	5.6	1.8	43.1		
58-34	RTFO	-24	1.4	2.0	14.7
			5.6	2.1	19.9
		-30	1.4	2.2	15.8
	5.6		2.3	20.5	
	PAV	-24	1.4	2.2	17.9
			5.6	1.9	20.5
-30		1.4	2.2	20.4	
	5.6	2.2	28.1		

Table 19. DTT asphalt binder experimental design and test results

Binder PG	Aging	Temperature (°C)	Mean Strength (MPa)	CV (%)
58-28	RTFOT	-18	4.4	8.6
		-24	4.8	12.6
	PAV	-18	4.2	13.9
		-24	4.2	30.8
58-34	RTFOT	-24	5.0	4.6
		-30	6.6	13.8
	PAV	-24	5.2	19.1
		-30	6.1	13.2

The results obtained on asphalt binder PG58-34 and PG58-28 clearly show that there is a significant difference between the values measured with BBR and DTT. However, the two tests are performed under different types of loading, three-point bending and direct tension, and the volumes of the specimens are significantly different: 9921.9mm³ and 1945.9mm³ for BBR and DTT, respectively. The dependence of structural strength on the structure size and geometry can be explained using the well-established size effect theory.

BBR and DTT specimens share the same failure mechanism, where the peak load is reached once a macro-crack initiates from one representative volume element (RVE). Therefore, the structure can be statistically represented by a chain of RVEs. The failure probability can be further calculated based on the joint probability theorem:

$$1 - P_f = \prod_{i=1}^n [1 - P_1(\sigma_i)] \quad [19]$$

or

$$\ln(1 - P_f) = \sum_{i=1}^n \ln[1 - P_1(\sigma_i)] \quad [20]$$

where

- P_f failure probability of the entire structure,
- P_1 failure probability of one RVE, and
- σ_i maximum principal stress at center of the i^{th} RVE.

RVE plays a major role in the calculation. It has been shown that the RVE size is roughly equal to 2-3 times of the size of material inhomogeneity or grain size (Bažant and Pang, 2007). In the present study, the grain size of the binder is on the micro-scale. Therefore, we may assume that the RVE size is almost negligible compared to the specimen size. Based on equation [5], what matters for the failure probability of the structure is the tail part of the strength distribution of one RVE.

Recent studies (Bažant *et al.*, 2009; Le *et al.*, 2011) showed that, based on atomistic fracture mechanics and on statistical multiscale transition framework, the tail of the strength

distribution of one RVE must follow a power-law , i.e. $P_I = (\sigma_i / s_0)^m$ (Bažant and Pang, 2007). Furthermore, by using the approximation $\ln(1-x) = -x$ for small value of x , we can re-write equation [20] as:

$$P_f = 1 - \exp\left\{-\sum_{i=1}^n [s(x_i)]^m (\sigma_N / s_0)^m\right\} \quad [21]$$

where

- $s(x_i)$ dimensionless stress field such that $\sigma_i = s(x_i)\sigma_N$,
- σ_N , nominal strength,
- s_0 material constant (scale parameter),
- m material constant called Weibull modulus (or shape parameter).

Since the structure size is much larger than the RVE size, the sum can be replaced by an integral over the volume V of the specimen:

$$P_f = 1 - \exp\left\{-\int_V [s(x)]^m dV(x)\right\} (\sigma_N / s_0)^m \quad [22]$$

Equation [8] indicates that the strength distribution would follow the classical two-parameter Weibull distribution (Rinne, 2009). By using simple elastic stress field for BBR and DTT, we can relate the mean strength of BBR specimen σ_N^B and the mean strength of DTT specimen σ_N^U

$$\frac{\sigma_N^B}{\sigma_N^U} = \left[4 \cdot (1+m)^2\right]^{1/m} \left(\frac{V_U}{V_B}\right)^{1/m} \quad [23]$$

where V_U and V_B are volume of DTT and BBR specimens, respectively. Using equation [23], we can predict the strength of DTT specimens from the strength of BBR specimens, where the Weibull modulus, m , is chosen to be about 10 based on the preliminary tests on strength histogram. Table 20 shows the comparison between predicted and measured DTT strengths.

Table 20. Comparison between DTT vs. BBR asphalt binder strength

Binder	Aging	T (°C)	Measured Mean Strength (MPa)		Ratio (%)	Corrected Mean Strength (MPa)	
			BBR	DTT		BBR to DTT	
PG58-28	PAV	-18	2.1	4.2	51.3	1.4	32.6
PG58-34	PAV	-24	1.9	5.2	35.5	1.2	22.5

It is clear that the predicted DTT strength is three to four times lower than the measured one and other factor(s) are responsible for the significant difference. The other significant difference between DTT and BBR tests is the cooling medium: DTT specimens are cooled using potassium acetate and BBR specimens are cooled using ethanol. Based on previous research conducted by Dongre and D'Angelo (1998), in which the authors showed that DTT strength in

ethanol is 3 to 5 times lower than DTT strength in potassium acetate or air, it was decided to investigate if cooling medium could cause such a significant effect on the structural strength.

Effect of cooling medium on BBR strength

In order to determine whether cooling fluid affects the failure response of asphalt binder when tested in three-point bending with BBR, a new set of experiments was performed on PG64-22 binder in RTFOT condition. BBR strength tests were run in ethanol and then in potassium acetate at PG - 2°C. From the nominal stress strain curves in Figure 68, it is evident that BBR mean strength in potassium acetate is almost 4.5 times higher than BBR mean strength in ethanol. Also, a small decrease in the stiffness of the binder is observed for the specimens tested in ethanol.

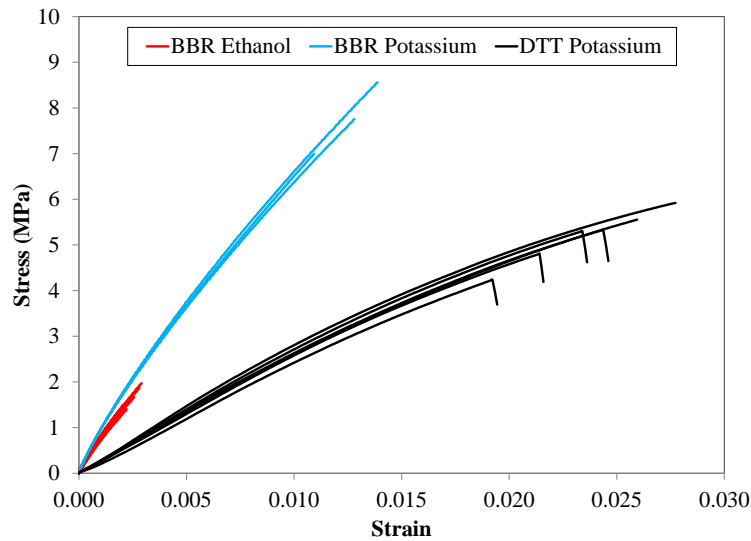


Figure 68. Cooling medium effect on BBR stress strain curves for binder PG64-22

Using the same Weibull approach it is possible to estimate of corrected strength for the new test results. Table 21 summarizes the test results as well as the corrected values for the BBR strength in ethanol (E) and in potassium acetate (PA).

Table 21. BBR and DTT results and comparison for different cooling media

Test	Rep.	Cooling Medium	Loading Rate	Mean Strength	Corrected BBR Mean Strength	Corrected BBR mean strength / DTT mean strength
Type	#		N/min	(MPa)	(MPa)	%
BBR-E	5	Ethanol	7.2	1.7	1.0	18.4
BBR-PA	3	Potassium Acetate	24	7.8	4.8	85.1
DTT	4	Potassium Acetate	-	5.7	-	

The corrected BBR strength in ethanol is almost five times smaller than DTT strength, while the corrected BBR strength in potassium acetate is fairly similar to DDT strength, since the 15% difference is less than testing variability.

The effect of cooling medium on BBR strength was further evaluated for binders PG58-28 and PG64-22, using the same loading rate (7.2N/min) and same testing temperature ($T = -24^{\circ}\text{C}$). The results in Table 22 provide further evidence of the strong effect of ethanol on the flexural strength, with a very similar impact on both asphalt binders (21-22% in ratio).

Table 22. Effect of cooling medium on BBR strength

Binder	Ethanol Mean Strength (MPa)	Potassium Acetate Mean Strength (MPa)	Ethanol - Potassium Acetate Mean Strength Ratio (%)
PG58-28	1.4	6.6	21.7
PG64-22	1.7	7.5	22.3

Many glassy polymers when exposed to organic solvents may fail at stresses and strains much lower than their normal values, if an adverse environment is present (Kambour, 1973; May, 1975). This is known in polymer literature as environmental stress cracking (ESC). Based on literature review, it can be hypothesized that both chemical interaction (with ethanol) and diffusion occurred in the asphalt binders specimens conditioned and tested in ethanol. This hypothesis needs to be further investigated and proved.

Conditioning and testing binder specimens in air appears to be a simple solution to this issue. However, asphalt binders are highly temperature susceptible materials and rigorous temperature control in air is much more difficult to achieve than in fluid. On-going research is addressing this challenge.